RSC Pharmaceutics

ROYAL SOCIETY OF CHEMISTRY

PAPER

View Article Online
View Journal | View Issue

Cite this: *RSC Pharm.*, 2025, **2**, 387

Sugar-decorated cholesterol-core nanoparticles as potential targeting nanomedicines for the delivery of lipophilic drugs†

Laís Rossetto Ferraz de Barros,[a] Carlos Eduardo de Castro,[a] Anabella Patricia Rosso,[a] Rodrigo da Costa Duarte,[b] Alexandre Gonçalves Dal-Bó,[b] Wendel Andrade Alves [a] and Fernando Carlos Giacomelli *[a]

Targeted drug delivery is a precise and effective strategy in oncotherapy and can be achieved through sugar-decorated assemblies since glucose receptors are overexpressed on cancer cell membranes to compensate for their increased glucose demands. In this study, core–shell nanoparticles (NPs) were synthesized using amphiphilic macromolecules comprising hydrophobic cholesterol (Chol) segments conjugated to hydrophilic polyethylene oxide containing azide group (Chol-PEO_{22}-N_3) or substituted with the carbohydrate *N*-acetyl-D-glucosamine (Chol-PEO_{22}-GlcNAc) *via* a click chemistry reaction. These self-assemblies, which are smaller than 100 nm and suitable for cancer treatment, demonstrated efficient loading efficiency (exceeding 70%) with ursolic acid (UA), a hydrophobic drug, serving as a proof-of-concept for targeted therapy using natural compounds against non-small cell lung cancer. The incorporation of sugar molecules modified the structural characteristics of the nanocarriers, resulting in larger and presumably less dense particles. This modification influenced the UA release mechanism, leading to a faster and nearly complete release over a week, whereas approximately 60% of the encapsulated UA remained entrapped in the Chol-PEO_{22}-N_3 NPs. Enhanced cell cytotoxicity was achieved with UA-loaded NPs with *in vitro* cell viability assays indicating at least two-fold increase in the inhibitory effect of the drug-loaded nanocarriers. The targeted delivery was also demonstrated as UA-loaded Chol-PEO_{22}-GlcNAc NPs showed greater internalization by cancer cells than their healthy counterparts.

Received 14th November 2024,
Accepted 19th January 2025

DOI: 10.1039/d4pm00317a

rsc.li/RSCPharma

1. Introduction

Cancer is a significant public health concern worldwide, causing approximately 1700 deaths per day in the United States[1] and more than 600 deaths per day in Brazil.[2] Among the different types of cancer, lung cancer usually remains the first or second leading cause of cancer death in both men and women every year,[1] and non-small cell lung cancer (NSCLC), which constitutes 80–85% of lung cancer cases, was selected as the model for this investigation. Chemotherapy is the primary approach for treating tumors and to mitigate its adverse effect such as cytotoxicity and limited selectivity, the development of nanotherapeutic platforms for cancer drug delivery has been proposed, aiming to enhance specificity and improve therapeutic efficacy.[3,4]

The enhanced permeability and retention (EPR) effect[5] allows nanoparticles (NPs) sized from 50 to 100 nm to accumulate more in tumor sites because of the imperfect architecture and irregular morphology of blood vessels in such locations. Furthermore, previous investigations have indicated that drug-loaded nanocarriers can be deposited and evade mucociliary clearance and alveolar macrophages in the lung-lining liquid, and clearance by alveolar macrophages is slower for relatively small particles (<80 nm).[6,7] Additionally, the cellular uptake process is crucial, as treatment efficiency often relies on the internalization of therapeutic agents. The surface chemistry of drug-loaded nanocarriers significantly influences nanoparticle–cell membrane interactions.[8] In this framework, polymer chains such as polyethylene oxide (PEO) can be used for biocompatibility and further functionalization, allowing the manufacturing of nanocarriers with targeting attributes and increased accumulation at a desired location. Small molecules can be conjugated to PEO chains through click reactions using organic azide, ensuring high-efficiency coupling in

[a]*Centro de Ciências Naturais e Humanas, Universidade Federal do ABC, 09210-580 Santo André, Brazil. E-mail: fernando.giacomelli@ufabc.edu.br*
[b]*Universidade do Extremo Sul Catarinense – UNESC, 88806-000 Criciúma, SC, Brazil*

† Electronic supplementary information (ESI) available. See DOI: https://doi.org/10.1039/d4pm00317a

aqueous environments.[9,10] In this context, short-chain carbohydrates (sugars) are being employed in the synthesis of targeted cargo delivery systems.[11,12] Glycidic moieties, for instance, have a high affinity for cell membrane components such as lecithins, thus promoting increased cellular uptake.[13] Sugars are particularly attractive as cancer-targeting ligands due to the augmented glycolysis in proliferating cancer cells, which leads to higher glucose uptake.[14,15] Since glucose receptors are overexpressed on cancer cell membranes, galactose, mannose, and glucose monosaccharide derivatives such as *N*-acetyl glucosamine serve as promising targeting ligands.[11,16]

Taking these considerations into account, we have evaluated two amphiphilic macromolecules: one with a hydrophobic fraction of cholesterol (to allow hydrophobic drug loading) conjugated to PEO terminated with an azide group (Chol-PEO_{22}-N_3) and the other with a PEO substituted with the carbohydrate (targeting ligand) *N*-acetyl glucosamine (Chol-PEO_{22}-GlcNAc). *N*-Acetylglucosamine (GlcNAc), which is an amide derivative of glucose, has been selected as the targeting ligand due to the enhanced metabolism, high glucose demand of cancer cells and amplified expression of glucose transporters in tumor sites.[17] These amphiphilic macromolecules were self-assembled into core–shell NPs that have been evaluated as potential nanocarriers for ursolic acid (UA), a model hydrophobic chemotherapeutic drug. UA is a pharmacologically active, natural pentacyclic triterpene derived from fruits, herbs, and plants,[18] and it can regulate the proliferation, metastasis, angiogenesis, and apoptosis of tumor cells by acting on a variety of cytokines.[19] UA has a significant therapeutic effect on breast, lung, colorectal, liver, and prostate cancer, for instance.[20] Despite its promising properties,[18] the poor water-solubility, low intestinal mucosal absorption, and low bioavailability restrict its clinical application and *in vivo* administration. These drawbacks can be circumvented by using nanotechnology-based platforms to enable its pharmacological administration. Accordingly, herein UA-loaded cholesterol-core sugar-decorated NPs were evaluated as a proof-of-concept to improve drug solubility and bioavailability to treat non-small cell lung cancer. A549 cells were used as a model for *in vitro* biological assays. This investigation therefore relies on the manufacturing of UA-loaded nanocarriers and subsequent evaluation of their structural features, colloidal stability, drug release profile, cell cytotoxicity, and cellular uptake.

2. Materials and methods

2.1. Amphiphilic macromolecules and other chemicals

The amphiphile azide-poly(ethylene glycol)-cholesterol conjugate Chol-PEO_{22}-N_3 and the glycosurfactant *N*-acetyl-β-D-glucosaminyl-poly(ethylene glycol)-cholesterol conjugate Chol-PEO_{22}-GlcNAc were synthesized according to previously reported procedures[13,21–23] with the methodology described in the ESI† along with respective product characterization by FTIR and ^{13}C NMR. All solvents, coumarin-6, and UA were of analytical grade purchased from Sigma-Aldrich. The water used in sample preparation was pretreated with Milli-Q® Plus System (Millipore Corporation).

2.2. Preparation of the UA-loaded and coumarin-6-loaded NPs

The NPs produced using Chol-PEO_{22}-N_3 and Chol-PEO_{22}-GlcNAc were prepared by nanoprecipitation. In this process, 5.0 mg of amphiphilic macromolecules were dissolved in 2.0 mL of organic solvent mixture (THF : acetone 25 : 75 v/v). The formation of the NPs was subsequently induced by injecting the organic phase (1 mL min^{-1}) into 5.0 mL of water. The organic solvent was further evaporated at 30 °C for 48 h, and the final volume was adjusted to 5.0 mL. Negligible amounts of organic solvent at the final samples can be expected by using this protocol.[24] To produce drug-loaded NPs, 0.25 mg of UA (5% w/w) was added during amphiphile dissolution in the organic phase. Probe-loaded NPs were similarly produced using 0.01 mg of coumarin-6 (0.2% w/w).

2.3. Structural characterization of the NPs

Dynamic light scattering (DLS) data were acquired using an ALV/CGS-3 compact goniometer. The autocorrelation functions were collected in triplicate (30 s counting time), further averaged, and analyzed using the Cumulant method to determine the values of the mean relaxation time (τ), and the values of hydrodynamic radius (R_H) were further determined using the straightforward Stokes–Einstein relation. The Cumulant method also allows to probe the polydispersity index (PDI) of the samples (μ_2/Γ^2).

The electrophoretic mobility (U_E) of the colloidal materials was measured using a Zetasizer Nano-ZS ZEN 3600 instrument (Malvern Instruments). Each sample was measured five times with three sub runs of 30 s counting time. The values were further converted to ζ-potential (mV) using the Henry's equation and Smoluchowski approximation.

Cryo-TEM images were acquired at the Brazilian Nanotechnology National Laboratory (LNNano) using a Talos F200C (Thermo Fisher Scientific) high-resolution microscope at an accelerating voltage of 200 kV. Two microliters of each sample were loaded into 01895 – Lacey Carbon, 300 mesh copper electron microscopy grids (Electron Microscopy Science). Excess sample was removed by blotting for 3 s, and the grids were immediately plunged into liquid ethane. The specimens were stored in liquid nitrogen and transferred, under controlled conditions, to an autoloader cassette and then to a microscopic column for imaging.

2.4. Determination of UA loading content (LC) and loading efficiency (LE)

The UA loading efficiency was determined by phase separation using Amicon® Ultra-15 centrifuge tubes (Merck Millipore, 10 000 MWCO). One milliliter of the drug-loaded NPs was placed in the reservoirs and centrifuged at 20 °C for 5 min and 5000 rpm. The volume of the filtrate was then set to 1.0 mL using a 8 : 2 v/v mixture of MeOH : water. This solvent mixture was selected in order to disassemble the core–shell nano-

particles. The UV-Vis absorbance of the filtrates was subsequently measured in triplicate (averaged values are provided) at λ = 200 nm (the maximum absorbance of UA) using a Varian Cary 50 Bio UV-Vis spectrophotometer. To determine the concentrations of UA, an analytical curve was generated with linear response (R^2 = 0.99) in the range 0.005–0.25 mg mL^{-1} in the same medium. The values of loading content (LC) and loading efficiency (LE) were calculated by using the following equations:

$$\text{LC}\,(\%) = \frac{\text{UA in NPs}}{\text{mass of NPs}} \times 100 \quad (1)$$

$$\text{LE}\,(\%) = \frac{\text{UA in NPs}}{\text{UA feeding}} \times 100 \quad (2)$$

2.5. Evaluation of UA release kinetics

UA release kinetics were evaluated using cellulose dialysis membranes (MWCO 8–10 kDa, Spectra-Por® Float-A-Lyzer® G2) using well-established protocols regularly used by us[25–27] as well as by other research groups.[28,29] The tubes were filled with 5.0 mL of the UA-loaded NPs and immersed in 2 L of phosphate-buffered saline (PBS) solution at pH 7.4 and 37 °C with gentle stirring. At predetermined times, 80 μL of the samples were removed from the dialysis tube and diluted with 320 μL of MeOH to determine the quantity of UA remaining in the samples. An equal volume of nanoparticle suspension was immediately replaced. The remaining amount of UA was determined by measuring the UV-Vis absorbance acquired in triplicate (averaged values are provided) at λ = 200 nm (the maximum absorbance of UA) using a Varian Cary 50 Bio UV-Vis spectrophotometer. Concentrations were calculated based on the calibration curve described in the previous section. The UA release kinetics were evaluated using different kinetic models: zero-order, first-order, Higuchi, and Korsmeyer-Peppas, as discussed in the Results and discussion sections.

2.6. Biological assays

2.6.1. Cell culture. MRC-5 cells (a kind gift from Princeton University, USA) were cultured in Dulbecco's modified Eagle's medium (DMEM), and A549 cells (a kind gift from AC Camargo Cancer Center, Brazil) were cultured in Dulbecco's modified Eagle's medium/nutrient mixture F-12 (DMEM/F-12, GlutaMAX supplement). The culture medium was supplemented with 10% fetal bovine serum (FBS), 10 000 U mL^{-1} penicillin, and 10 000 μg mL^{-1} streptomycin at 37 °C under CO_2 atmosphere.

2.6.2. Cytotoxicity assay. The viability of A549 and MRC-5 cells was evaluated in the concentration range 5–50 μg mL^{-1} using 1 × 10^4 cells per well that were shown in 96-well plate culture for 24 h at 37 °C. Subsequently, the cells were treated with DMEM with the addition of 50 μL of NPs and incubated for 24 h at 37 °C. Then, the wells were washed with PBS, and 50 μL per well of thiazolyl blue tetrazolium bromide (Sigma-Aldrich) was added at 0.3 mg mL^{-1}. The plates were incubated for 2 h at 37 °C. Subsequently, 150 μL per well of dimethyl sulfoxide (DMSO) was added, the plate was shaken for 15 min, and the absorbance of the plate was determined at 570 nm using a Synergy microplate reader. The experiments were conducted in triplicate, and cell viability was determined relative to the untreated controls. Statistical analysis was performed using two-way ANOVA followed by Bonferroni's multiple comparison test. Differences were considered statistically significant for p values <0.05.

2.6.3. Cellular uptake. A549 and MRC-5 cells (1 × 10^4 cells per well) were cultured in 24-well plates for 24 h, then the cell culture medium was replaced by 380 μL of fresh FBS-free DMEM with the addition of 20 μL of coumarin-6 loaded NPs. After 1 h incubation at 37 °C, cells were washed three times with PBS and fixed with 4% paraformaldehyde for 10 min. The nuclei and membranes of the cells were labeled with 30 μL of DAPI and 6 μL of rhodamine, respectively. Qualitative analysis of the cellular uptake was performed using a wide-field Leica DMI 6000 B microscope (Leica Microsystems, Wetzlar, Germany) coupled to an ultrafast Leica DFC365 FX digital camera. Filter cube L5 (excitation, 460–500 nm; DC 505; emission, 512–542 nm) was selected to acquire green fluorescence (coumarin-6). Images were obtained at 63× magnitude, and data treatment was performed using ImageJ software.

The cellular uptake of the NPs was further quantified by flow cytometry analysis using essentially the same procedures described above, except that 1 × 10^4 cells per well were plated, incubated for 1 h, washed three times with PBS, harvested by trypsinization using trypsin–EDTA solution, fixed with 4% paraformaldehyde for 10 min, and finally resuspended. Measurements were performed using a BD FACS Canto II flow cytometer (using a FITC filter for coumarin-6) and analyzed using the FlowJo V.6 software. Flow cytometry analyses were performed in triplicate (10 000 events were collected for each experiment), and the data are presented as the mean ± standard deviation. Statistical analyses were performed using a one-way ANOVA followed by Tukey's test. A p-value of 0.05 or greater was considered statistically significant.

3. Results and discussion

3.1. Synthesis of the amphiphilic macromolecules

The synthetic strategy used to prepare the amphiphile azide-poly(ethylene oxide)-cholesterol conjugate Chol-PEO$_{22}$-N$_3$ (**2**) from the initial reactant cholesteryl hemisuccinate (**1**) and the glycosurfactant *N*-acetyl-β-D-glucosaminyl-poly(ethylene oxide)-cholesterol conjugate Chol-PEO$_{22}$-GlcNAc (**3**) is illustrated in Fig. 1.

The synthesis of the amphiphilic macromolecules has been detailed in previous publications.[13,21–23] Briefly, the hemisuccinate cholesteryl group was conjugated to the PEO chains *via* an esterification reaction using dicyclohexylcarbodiimide (DCC), resulting in a 72% yield of "ready-to-click" Chol-PEO$_{22}$-N$_3$. Propargyl β glycosides of *N*-acetyl-glucosamine were further introduced at the polar head of the surfactant *via* copper-cata-

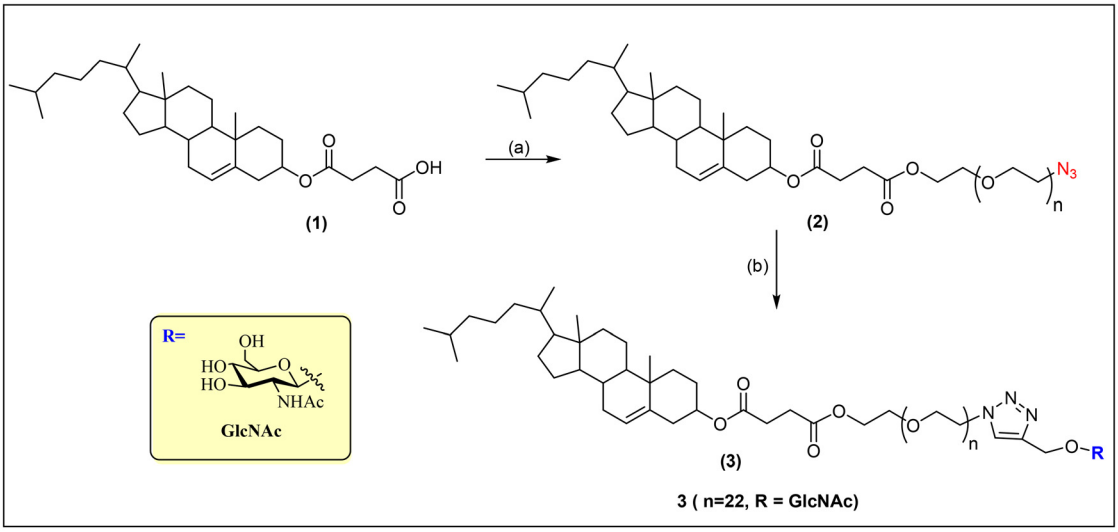

Fig. 1 Synthetic strategy used in the preparation of (**2**) azide-poly(ethylene oxide)-cholesterol conjugate Chol-PEO_{22}-N_3 and (**3**) glycosurfactant *N*-acetyl-β-D-glucosaminyl-poly(ethylene glycol)-cholesterol conjugate Chol-PEO_{22}-GlcNAc: (a) *N*,*N*′-dicyclohexylcarbodiimide (DCC), 4-dimethylaminopyridine (DMAP), mono-azide-PEO (PEO_{22}-N_3), CH_2Cl_2, 72%; (b) copper sulfate ($CuSO_4$), sodium ascorbate ($C_6H_7O_6Na$), propargyl-2-*N*-acetamido-2-deoxy-β-D-glucopyranoside ($C_7H_{17}NO_6$, H_2O/THF, 70%).

lyzed azide–alkyne Huisgen cycloaddition. The reaction was carried out at 40 °C with copper/ascorbate as a catalyst in a water/THF mixture to ensure good solubility of the amphiphile. The glycosylated conjugate Chol-PEO_{22}-GlcNAc was isolated in 70% yield after purification by silica gel chromatography. Characterization of the amphiphiles was conducted using FTIR and ^{13}C NMR analyses, where the characteristic signals of the aliphatic chains, ethylene oxide, and the carbohydrate unit, as well as the signals of the triazolyl ring, were identified. These experimental data are provided in the ESI (Fig. S1–S4†) along with further details of the employed synthetic approach.

3.2. Manufacturing and structural characterization of the nanocarriers

Dynamic light scattering (DLS) autocorrelation functions and respective size distributions for the produced amphiphilic NPs are shown in Fig. 2, highlighting sub-100 nm self-assemblies with sizes ranging from 36 to 79 nm.

Table 1 lists the quantitative data. The sizes of the nanocarriers are suitable for cancer treatment as they are larger than the threshold for fast renal clearance ($D_H = 2R_H >$ 10 nm)[30,31] and smaller than 100 nm, which is the average pore size of tumor sites, enabling enhanced accumulation *via* the EPR effect.[5,32] The particle size increases with UA (5% w/w) loading, reflecting changes in the internal structure of the nanocarriers,[33] and the surface charge is possibly the results of ionized groups (probably hydroxide ions) at the interface between water and the organic shells.[34] The UA loading does not significantly affect the surface charge of the NPs.

The negative zeta potential of the assemblies is expected to provide enhanced colloidal stability. Furthermore, positively charged NPs may indeed induce fast nanoparticle clearance due to protein adsorption whereas negative surfaces can impart protein-repelling features since main protein components at the bloodstream are negatively charge at physiological pH, thus enabling longer blood circulation time. The surface charge, size and size distribution of the manufactured soft colloids have been frequently checked over 4 months and no signs of nanoparticle aggregation when stored at 4 °C have been detected. Due to the presence of fairly negative values of ζ-potential, the colloidal stability is supposed to come at least partially from electrostatic effects since repulsive Coulomb forces acting between the charged colloidal particles are certainly present.

Morphological observations through cryo-TEM (Fig. 3) showed homogenous and spherical structures in reasonable agreement with the size range obtained by DLS. The images confirm also the formation of NPs in the presence of UA.

Differences regarding in the cryo-TEM images may be the result of disparate electron density contrast in the presence and in the absence of UA nevertheless, core–shell structures are more likely to be produced taking into account the weight fraction of the hydrophobic segment (roughly 30%). Additionally, discrepancies when comparing cryo-TEM and DLS data are to some extent acceptable since light scattering intensity is heavily weighted by the particle size implying that DLS is particularly sensitive to larger compared to smaller scattering objects.

3.3. Evaluation of UA loading content (LC) and loading efficiency (LE)

The determined values of UA loading content (LC) and loading efficiency (LE) are listed in Table 2. The experimental data show that UA was encapsulated to a slightly greater extent in Chol-PEO_{22}-GlcNAc NPs, possibly reflecting the larger

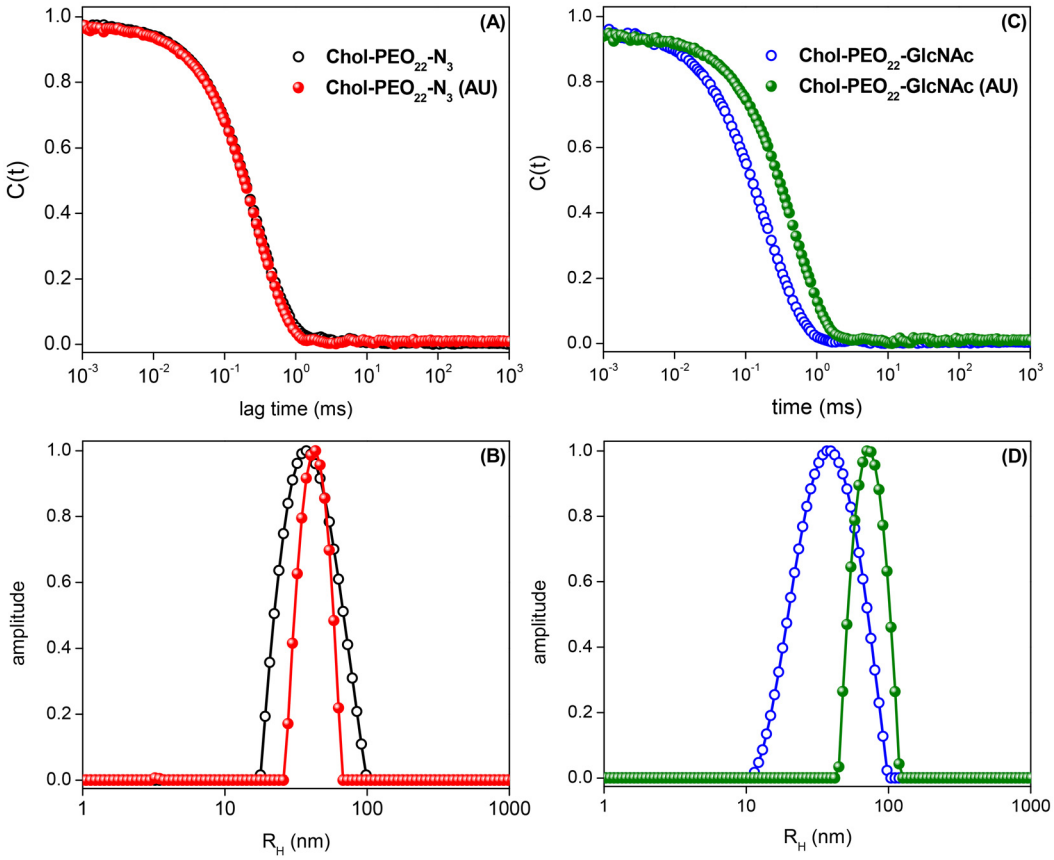

Fig. 2 Dynamic light scattering data acquired for drug-free and 5% w/w UA-loaded Chol-PEO_{22}-N_3 and Chol-PEO_{22}-GlcNAc NPs: (A and C) auto-correlation functions and (B and D) respective distributions of sizes.

Table 1 Structural characteristics of the unloaded and UA-loaded amphiphilic NPs as determined by light scattering techniques

Nanoparticle	R_H (nm)	PDI	ζ (mV)
Chol-PEO_{22}-N_3	40	0.37	−25.1 ± 0.8
Chol-PEO_{22}-N_3 (UA)	48	0.20	−22.5 ± 0.7
Chol-PEO_{22}-GlcNAc	36	0.47	−19.2 ± 0.7
Chol-PEO_{22}-GlcNAc (UA)	79	0.22	−22 ± 1

volume of these nanocarriers. However, the size of the UA-loaded Chol-PEO_{22}-GlcNAc (Table 1) was probably balanced by a lower particle density; therefore, the LE and LC values were not significantly different.

The LE is approximately 70–80%, which is higher than values reported for UA loaded into other assemblies, such as dendrimer-like NPs (UA-G4K)[33] or poly(lactic-*co*-glycolic acid)-*b*-polyethylene glycol diblock copolymer NPs.[35] The LE for Chol-PEO_{22}-GlcNAc NPs is similar to that reported for chitosan NPs cross-linked with sodium tripolyphosphate.[36] High LE values are hardly achieved during UA loading,[19] making this an outstanding feature of the investigated systems, possibly due to the high degree of core hydrophobicity and therefore, favorable core–drug intermolecular interactions. The UA water solubility is equal to 0.005 mg mL^{-1}.[33–35] Considering the values of LC and LE reported in Table 2, the UA solubility in the formulated samples is approximately 40 times higher than as free drug. Because of its high degree of hydrophobicity, which contributes to its affinity for nonpolar organic solvents, UA migrates towards the cholesteric hydrophobic cores of the assemblies during nanoprecipitation. Thus, this method has proven efficient in developing cargo delivery systems aimed at increasing the solubility of lipophilic drugs for systemic administration.[18]

3.4. *In vitro* release of UA

Subsequently, the UA release profiles were examined. Drug release from soft NPs may occur *via* dissolution, diffusion, partitioning, osmosis, swelling, or erosion.[37] The release mechanism can be understood using mathematical models to fit the experimental data. The cumulative release of UA was evaluated in PBS (pH 7.4), and the experimental data are shown in Fig. 4.

The UA release showed a biphasic pattern, with an initial rapid release from Chol-PEO_{22}-N_3 (up to 12 h), followed by slower release, achieving a maximum release of approximately 40%. In contrast, the drug release from Chol-PEO_{22}-GlcNAc NPs was initially rapid (up to 12 h) and then slower. However, it was faster than that for Chol-PEO_{22}-N_3 with nearly quantitat-

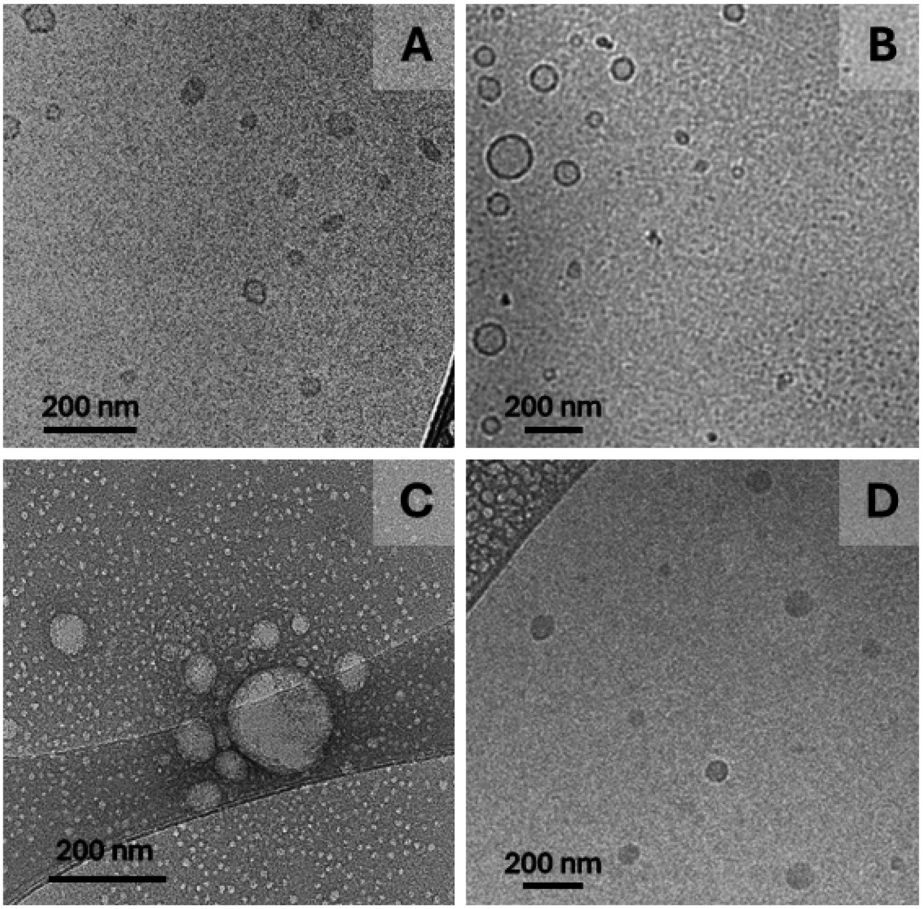

Fig. 3 Cryo-TEM images for (A) Chol-PEO_{22}-N_3 and (B) Chol-PEO_{22}-N_3 NPs loaded with 5% w/w UA, (C) Chol-PEO_{22}-GlcNAc and (D) Chol-PEO_{22}-GlcNAc NPs loaded with 5% w/w UA. The value of 5% w/w refers to the UA feeding.

Table 2 Values of UA loading efficiency and loading content for sugar-free and sugar-decorated amphiphilic NPs

Nanoparticle	LE (%)	LC (%)
Chol-PEO_{22}-N_3	71 ± 1	3.6 ± 0.1
Chol-PEO_{22}-GlcNAc	81 ± 2	4.1 ± 0.1

ive elution. This feature is remarkable because the complete release of UA was achieved from Chol-PEO_{22}-GlcNAc, whereas approximately 60% of UA remained encapsulated in the Chol-PEO_{22}-N_3 counterparts after a week. The larger size of UA-loaded Chol-PEO_{22}-GlcNAc NPs (Table 1) and the presence of the sugar moieties likely lead to greater swelling in the assemblies and lower particle density, facilitating the complete UA release. This sustained release over a week is desirable for targeted delivery at specific locations. To quantitatively evaluate the kinetics of UA release, the profiles in Fig. 4A were analyzed using zero-order, first-order, Higuchi, and Korsmeyer-Peppas models. Briefly, the zero-order model describes the drug release from NPs at a constant rate, independent of concentration. The first-order model indicates a release rate dependent on the remaining drug concentration. The Higuchi model addresses drug release from an insoluble matrix as the square root of a time-dependent process based on Fickian diffusion, whereas the Korsmeyer-Peppas model describes drug release from various systems, including Fickian and non-Fickian diffusion. This model is useful when the release mechanism is unknown, or when more than one type of drug release mechanism is involved.[37] The models are mathematically described by the following equations:

$$Q_t = Q_0 - K_0 t \quad (3)$$

$$\ln Q_t = \ln Q_0 - K_1 t \quad (4)$$

$$Q_t = K_H \sqrt{t} \quad (5)$$

$$\log Q_t = \log K_{KP} + n \log t \quad (6)$$

Q_t is the quantity of drug released at time t, and Q_0 is the initial quantity at t = 0 h. The zero-order, first-order, Higuchi, and Korsmeyer-Peppas constants are K_0, K_1, K_H, and K_{KP}, respectively. The suggested release mechanism is discussed based on the kinetic models and the values of R^2 reported in Table 3. These values suggest that the Korsmeyer-Peppas model provided the best fit for Chol-PEO_{22}-N_3 NPs, whereas the Higuchi model

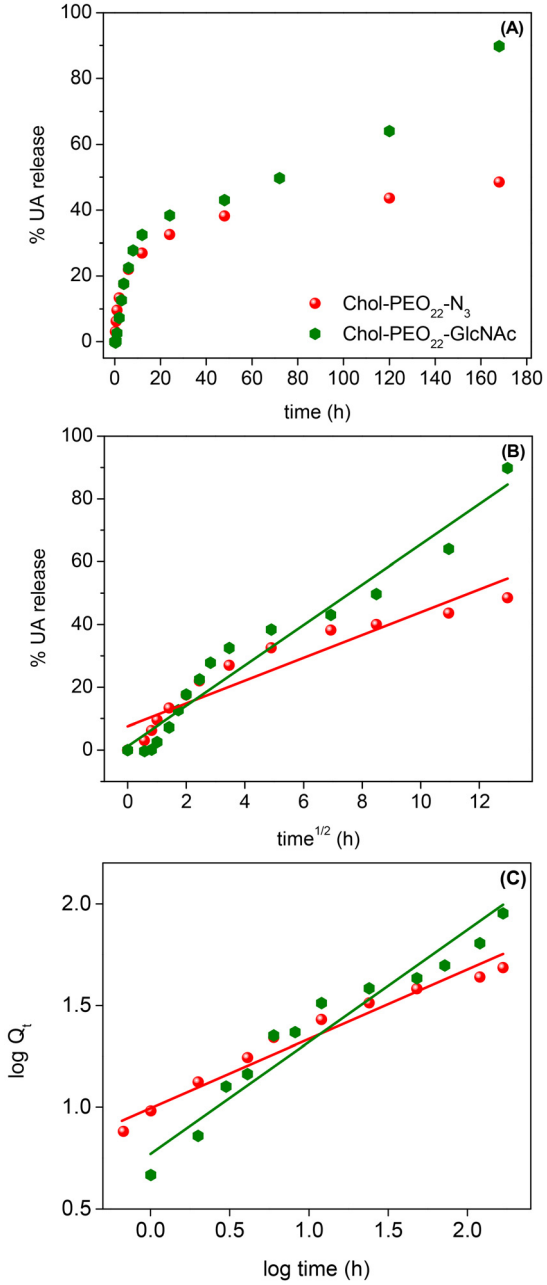

Fig. 4 (A) UA release profiles and UA release model fitting using the Higuchi (B) and the Korsmeyer-Peppas (C) approaches from Chol-PEO_{22}-N_3 and Chol-PEO_{22}-GlcNAc NPs.

was most suitable for Chol-PEO_{22}-GlcNAc NPs. However, the Korsmeyer-Peppas model showed relatively high R^2 values. The Higuchi and Korsmeyer-Peppas fittings are shown in Fig. 4B and C, and the others have been omitted for brevity.

In the Korsmeyer-Peppas plot, n (eqn (6)) indicates the release exponent, and this value indicates the mechanism of drug release. For spherical particles, $n \leq 0.43$ suggests drug release *via* Fickian diffusion, and values of $0.43 < n < 0.85$ indicate anomalous transport that usually occurs due to a combination of diffusion and erosion processes; for $n \geq 0.85$, the

Table 3 Fitting parameters as obtained using different mathematical models to evaluate UA release kinetics from the different amphiphilic NPs

Parameter	Chol-PEO_{22}-N_3	Chol-PEO_{22}-GlcNAc
Zero-order		
r^2	0.65	0.85
K_0 (h^{-1})	0.24 ± 0.05	0.48 ± 0.05
First-order		
r^2	0.37	0.24
K_1 (h^{-1})	0.010 ± 0.004	0.018 ± 0.008
Higuchi		
r^2	0.87	**0.95**
K_H ($h^{-1/2}$)	3.6 ± 0.4	**6.4 ± 0.4**
Korsmeyer-Peppas		
r^2	**0.96**	0.93
N	**0.33**	0.51
K_{KP} (h^{-n})	**10.4**	6.6

erosion mechanism is dominant.[37] The value of n = 0.33 for Chol-PEO_{22}-N_3 (Table 3) suggests UA release dominated by a Fickian diffusion, while UA release from Chol-PEO_{22}-GlcNAc fits better with the Higuchi model, indicating drug release occurring through the porosity of the matrix,[37] resulting in

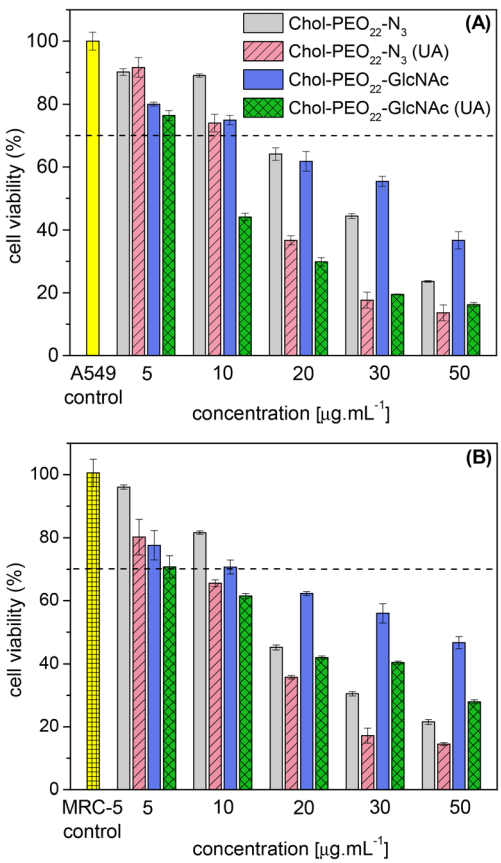

Fig. 5 Viability of (A) A549 and (B) MRC-5 cells after 24 h exposure to various concentrations of NPs. The results were normalized to 100% viability from control cells ($n \geq 3$).

negligible matrix dissolution and constant drug diffusion. The differing release mechanisms likely result from the size of the NPs, with larger Chol-PEO_{22}-GlcNAc NPs having a lower particle density and a higher surface-to-volume ratio compared to their counterparts.

3.5. Biological assays

3.5.1. Evaluation of *in vitro* cell viability. Cell viability assays were conducted using non-tumor lung fibroblasts (MRC-5) and the lung tumor cell line A549. The 3-(4,5-dimethylthiazolyl-2)-2,5-diphenyltetrazolium bromide (MTT)

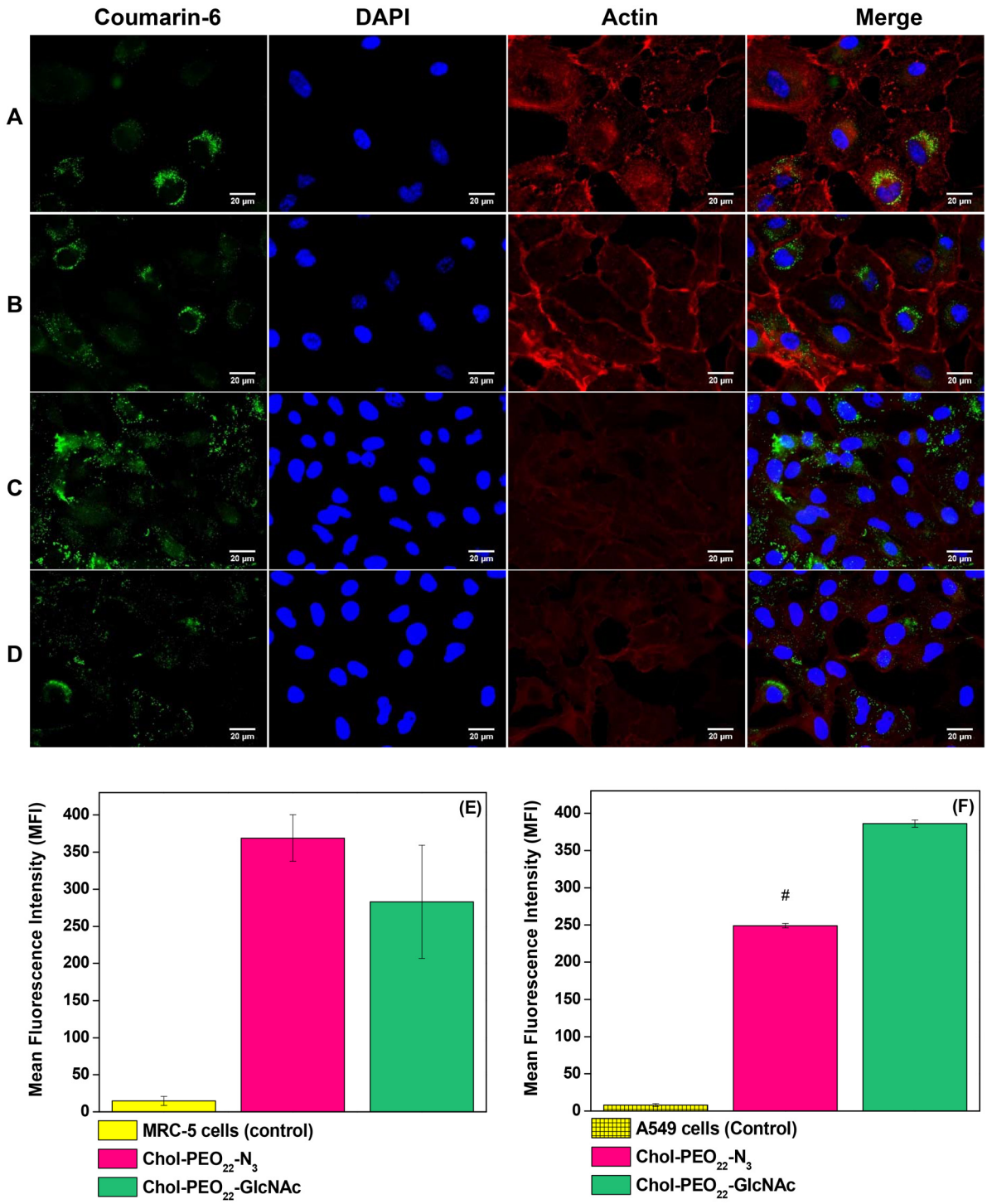

Fig. 6 (Top) Fluorescence microscopy images of MRC-5 cells incubated for 1 h with coumarin-6-loaded (A) Chol-PEO_{22}-GlcNAc and (B) Chol-PEO_{22}-N_3 NPs; A549 cells incubated for 1 h with coumarin-6-loaded (C) Chol-PEO_{22}-GlcNAc and (D) Chol-PEO_{22}-N_3 NPs. (Bottom) Flow cytometry data (mean fluorescence intensity – MFI) for (E) MRC-5 and (F) A549 cells incubated for 1 h with coumarin-6-loaded NPs.

assays indicated that the cells are viable up to a concentration of 10 μg mL^{-1}, regardless of the phenotype (Fig. 5), consistent with reported values for different surfactants used in cell biology.[38] Detailed statistical analysis of such set of data are provided in the ESI (Fig. S5†). The protective effect of the sugar moieties is evident since they are well tolerated by living systems.[39] Although at higher concentrations the cell viability is notably reduced also for the NPs themselves, the sugar-decorated assemblies are demonstrated to be always less cytotoxic. Furthermore, at the mid-range concentration, remarkable different values of cell viability were monitored for drug-free and UA-loaded NPs (especially for Chol-PEO_{22}-GlcNAc at 10 μg mL^{-1}) particularly for A549 cells which therefore highlights their potential application as cargo delivery system with targeting attributes. The presence of naked azide groups leads to a more pronounced cytotoxic effect since such a chemical entity is used to inhibit cell metabolism.[40]

When the ISO 10993 5:2009 standard is considered, cytotoxic effects are considered when the cell viability is reduced by more than 30% compared to the control (untreated cells). In this regard, drug-free NPs are non-toxic at concentrations of 5 μg mL^{-1} and 10 μg mL^{-1}, while UA-loaded NPs are not cytotoxic only if administered at a maximum concentration of 5 μg mL^{-1}. The experimental data indeed clearly confirms that the UA loaded into the NPs promotes an additive cytotoxic effect.

Furthermore, when the different phenotypes are considered, there is a notably enhanced reduction in cell viability particularly for UA-lading Chol-PEO_{22}-GlcNAc in contact with A549 cells. This can be seen, for instance, by comparing the experimental data at 30 μg mL^{-1}. Accordingly, the presence of sugar-decorated particles reduces the toxicity of the NPs and, simultaneously, it promotes a higher cytotoxicity selectively for lung tumor A549 cells in the presence of the natural active agent.

3.5.2. *In vitro* cellular uptake. The cellular uptake of the amphiphilic NPs by MRC-5 and A549 cells was further evaluated. Since we cannot track the cellular uptake of the NPs by fluorescence microscopy and flow cytometry with loaded UA, these experiments have been performed using a small amount of loaded coumarin-6. We have indeed previously used such protocol to track the cellular internalization of nanoparticles by using this fluorescent probe.[41,42] Furthermore, coumarin-6 having water solubility similar to that of antitumor agents such as paclitaxel, serves as a practical model for the transport and release of hydrophobic drugs. The microscopy images shown in Fig. 6 indicate the presence of NPs diffused in the cell cytoplasm, pointing out low partitioning of the assemblies in the cell membrane. Furthermore, the absence of green fluorescence in the cell nuclei, possibly because of the limited pore size (approximately 12 nm), restricts nanoparticle diffusion towards the nucleus of the cells and suggests NP accumulation in endocytic vesicular structures, implying endocytic uptake pathways[31] and suggesting cytosolic delivery. The ursolic acid however targets numerous molecular players of different cell signaling cascades to promote its anti-cancer potential. Respectively, it does not need to be uptaken by the cell nuclei to exerts the active action.[20]

The mean fluorescence intensity (MFI) of flow cytometry data (Fig. 6E and F) revealed no significant difference in uptake between Chol-PEO_{22}-N_3 and Chol-PEO_{22}-GlcNAc NPs by MRC-5 cells. However, the MFI value for Chol-PEO_{22}-GlcNAc NPs was significantly higher than that for Chol-PEO_{22}-N_3 NPs in A549 cells. Because glucose transporters and lectin-like receptors are overexpressed in almost all tumor cells in lung tissues[11] these data suggest an increased affinity of sugar-decorated nanostructures to A549 cells. This characteristic is particularly significant for cancer therapy because tumor cells can internalize a higher quantity of sugar-decorated NPs, thereby minimizing off-target effects and enhancing therapeutic efficacy.

4. Conclusions

Herein, the manufacture of UA-loaded, sugar-decorated cholesterol-core NPs with less than 100 nm in size that are suitable for cancer treatment is reported. The nanocarriers demonstrated a high LE for UA (>70%) while maintaining colloidal stability. The *in vitro* cell viability assays indicated at least a two-fold increase in the inhibitory effect of the drug-loaded nanocarriers compared with their unloaded counterparts. Chol-PEO_{22}-GlcNAc NPs are larger and presumably less dense than their sugar-free assemblies, and such features enable a more rapid and complete release of the loaded UA within approximately one week. In contrast, approximately 60% of the loaded amount was still entrapped at the core of the sugar-free self-assemblies after 7 days. Furthermore, the Chol-PEO_{22}-GlcNAc NPs demonstrated targeted *in vitro* delivery, as they were internalized to a greater extent by A549 cancer cells compared to non-decorated NPs. These findings suggest significant potential for the development of advanced nanoplatforms for tumor therapy. The cholesterol core's ability to encapsulate highly hydrophobic drugs aligns with the properties of several chemotherapeutics, while the sugar molecules serve as effective ligands for targeting receptors overexpressed in cancer cells. This research article opens avenues for future studies to explore the therapeutic potential of sugar-decorated cholesterol-core nanoparticles across a broader range of cancer types and to investigate their *in vivo* efficacy and safety profiles. Additionally, further research could focus on optimizing the nanoparticle design to enhance targeted drug delivery and improve clinical outcomes in cancer treatment.

Data availability

The relevant data supporting this article have been included as part of the ESI.†

Conflicts of interest

The authors declare that they have no known competing financial interests or personal relationships that could have appeared to influence the work reported in this paper.

Acknowledgements

This work was supported by FAPESP (grants 2021/12071-6, 2022/14753-0 and 2023/00558-3), CNPq (grant no. 303268/2020-4 and 305574/2023-0), and the National Institute of Science and Technology in Bioanalytics-INCTBio (FAPESP grant 2014/50867-3 and CNPq grant 465389/2014-7). We thank CEM at UFABC for granting access to its light scattering facilities, and the LNNano (CNPEM, Brazil) is acknowledged for granting access to the cryo-TEM facilities (BAG proposal 20233074). A. P. R. acknowledges the scholarship granted by FAPESP (grant 2022/14668-2), and A. G. D. acknowledges financial support from FAPESC (grant 2023TR000872) and CNPq (grant 303985/2021-6).

References

1 R. L. Siegel, A. N. Giaquinto and A. Jemal, *Ca-Cancer J. Clin.*, 2024, **74**, 12–49.
2 Estatísticas de Câncer no Brasil, **https://www.inca.gov.br/numeros-de-cancer**.
3 P. Kumari, B. Ghosh and S. Biswas, *J. Drug Targeting*, 2016, **24**, 179–191.
4 H. Zhang, X. Li, J. Ding, H. Xu, X. Dai, Z. Hou, K. Zhang, K. Sun and W. Sun, *Int. J. Pharm.*, 2013, **441**, 261–268.
5 J. Fang, H. Nakamura and H. Maeda, *Adv. Drug Delivery Rev.*, 2011, **63**, 136–151.
6 I. M. El-Sherbiny, N. M. El-Baz and M. H. Yacoub, *Glob. Cardiol. Sci. Pract.*, 2015, **2015**, 2.
7 E. Lepeltier, C. Bourgaux and P. Couvreur, *Adv. Drug Delivery Rev.*, 2014, **71**, 86–97.
8 C. E. de Castro, C. A. S. Ribeiro, A. C. Alavarse, L. J. C. Albuquerque, M. C. C. da Silva, E. Jäger, F. Surman, V. Schmidt, C. Giacomelli and F. C. Giacomelli, *Langmuir*, 2018, **34**, 2180–2188.
9 S. Zhang, K. H. Chan, R. K. Prud'Homme and A. J. Link, *Mol. Pharm.*, 2012, **9**, 2228–2236.
10 H. Koo, S. Lee, J. H. Na, S. H. Kim, S. K. Hahn, K. Choi, I. C. Kwon, S. Y. Jeong and K. Kim, *Angew. Chem., Int. Ed.*, 2012, **51**, 11836–11840.
11 D. Pooja, T. Srinivasa Reddy, H. Kulhari, A. Kadari, D. J. Adams, V. Bansal and R. Sistla, *Eur. J. Pharm. Biopharm.*, 2020, **154**, 377–386.
12 H. Freichels, R. Jérôme and C. Jérôme, *Carbohydr. Polym.*, 2011, **86**, 1093–1106.
13 A. G. Dal Bó, V. Soldi, F. C. Giacomelli, B. Jean, I. Pignot-Paintrand, R. Borsali and S. Fort, *Soft Matter*, 2011, **7**, 3453–3461.
14 S.-G. Sampathkumar, M. B. Jones, M. A. Meledeo, C. T. Campbell, S. S. Choi, K. Hida, P. Gomutputra, A. Sheh, T. Gilmartin, S. R. Head and K. J. Yarema, *Chem. Biol.*, 2006, **13**, 1265–1275.
15 M. G. V. Heiden, L. C. Cantley and C. B. Thompson, *Science*, 2009, **324**, 1029–1033.
16 L. Lavín de Juan, V. García Recio, P. Jiménez López, T. Girbés Juan, M. Cordoba-Diaz and D. Cordoba-Diaz, *J. Drug Delivery Sci. Technol.*, 2017, **42**, 126–133.
17 S. Yan, J. Na, X. Liu and P. Wu, *Pharmaceutics*, 2024, **16**, 1–19.
18 L. Wang, Q. Yin, C. Liu, Y. Tang, C. Sun and J. Zhuang, *Front. Pharmacol.*, 2021, **12**, 706121.
19 A. Miatmoko, E. A. Mianing, R. Sari and E. Hendradi, *Front. Pharmacol.*, 2021, **12**, 1–19.
20 S. Zafar, K. Khan, A. Hafeez, M. Irfan, M. Armaghan, A. ur Rahman, E. S. Gürer, J. Sharifi-Rad, M. Butnariu, I. C. Bagiu and R. V. Bagiu, *Cancer Cell Int.*, 2022, **22**, 1–15.
21 Y. M. S. Micheletto, N. P. da Silveira, D. M. Barboza, M. C. dos Santos, V. R. de Lima, F. C. Giacomelli, J. C. V. Martinez, T. E. A. Frizon and A. G. D. Bó, *Colloids Surf., A*, 2015, **467**, 166–172.
22 A. G. Dal Bó, V. Soldi, F. C. Giacomelli, C. Travelet, R. Borsali and S. Fort, *Carbohydr. Res.*, 2014, **397**, 31–36.
23 M. Cardoso dos Santos, B. Silva de Farias, D. da Costa Cabrera, T. Roberto, St'. A. Cadaval Junior, L. Antonio de Almeida Pinto, A. Gonçalves Dal-Bó and V. R. de Lima, *Chem. Phys. Lipids*, 2021, **235**, 105027.
24 F. A. de Oliveira, L. J. C. Albuquerque, K. A. Riske, E. Jäger and F. C. Giacomelli, *J. Colloid Interface Sci.*, 2020, **574**, 260–271.
25 A. P. Rosso, F. A. de Oliveira, P. Guégan, E. Jager and F. C. Giacomelli, *J. Colloid Interface Sci.*, 2024, **671**, 88–99.
26 L. J. C. Albuquerque, V. Sincari, A. Jäger, J. Kucka, J. Humajova, J. Pankrac, P. Paral, T. Heizer, O. Janouškova, I. Davidovich, Y. Talmon, P. Pouckova, P. Štěpánek, L. Sefc, M. Hruby, F. C. Giacomelli and E. Jäger, *J. Controlled Release*, 2021, **332**, 529–538.
27 E. Jäger, P. Černoch, M. Vragovic, L. J. C. Albuquerque, V. Sincari, T. Heizer, A. Jäger, J. Kučka, O. Š. Janoušková, E. Pavlova, L. Šefc and F. C. Giacomelli, *Biomacromolecules*, 2024, **25**, 4192–4202.
28 C. Sanson, C. Schatz, J. F. Le Meins, A. Soum, J. Thévenot, E. Garanger and S. S. Lecommandoux, *J. Controlled Release*, 2010, **147**, 428–435.
29 J. S. Katz, K. A. Eisenbrown, E. D. Johnston, N. P. Kamat, J. Rawson, M. J. Therien, J. A. Burdick and D. A. Hammer, *Soft Matter*, 2012, **8**, 10853–10862.
30 A. Sánchez, S. P. Mejía and J. Orozco, *Molecules*, 2020, **25**, 1–45.
31 N. D. Donahue, H. Acar and S. Wilhelm, *Adv. Drug Delivery Rev.*, 2019, **143**, 68–96.
32 Y.-R. Zhang, R. Lin, H.-J. Li, W.-L. He, J.-Z. Du and J. Wang, *Wiley Interdiscip. Rev.: Nanomed. Nanobiotechnol.*, 2019, **11**, e1519.
33 S. Alfei, A. M. Schito and G. Zuccari, *Nanomaterials*, 2021, **11**, 2196.
34 L. S. McCarty and G. M. Whitesides, *Angew. Chem., Int. Ed.*, 2008, **47**, 2188–2207.
35 A. Markowski, A. Jaromin, P. Migdał, E. Olczak, A. Zygmunt, M. Zaremba-Czogalla, K. Pawlik and J. Gubernator, *Int. J. Mol. Sci.*, 2022, **23**, 5536.

36 L. Zhao, X. Duan, W. Cao, X. Ren, G. Ren, P. Liu and J. Chen, *Foods*, 2021, **10**, 2470.
37 M. L. B. T.-S. to M. the D. R. from P. S. Bruschi, Ed., Woodhead Publishing, 2015, pp. 63–86.
38 B. Arechabala, C. Coiffard, P. Rivalland, L. J. Coiffard and Y. de Roeck-Holtzhauer, *J. Appl. Toxicol.*, 1999, **19**, 163–165.
39 C. A. S. Ribeiro, L. J. C. Albuquerque, C. E. de Castro, B. L. Batista, A. L. M. de Souza, B. L. Albuquerque, M. S. Zilse, I. C. Bellettini and F. C. Giacomelli, *Colloids Surf., A*, 2019, **580**, 123690.
40 X. Zhang, A. Ji, Z. Wang, H. Lou, J. Li, L. Zheng, Y. Zhou, C. Qu, X. Liu, H. Chen and Z. Cheng, *J. Med. Chem.*, 2021, **64**, 11543–11553.
41 C. E. De Castro, C. A. S. Ribeiro, A. C. Alavarse, L. J. C. Albuquerque, M. C. C. Da Silva, E. Jäger, F. Surman, V. Schmidt, C. Giacomelli and F. C. Giacomelli, *Langmuir*, 2018, **34**, 2180–2188.
42 C. E. De Castro, C. A. S. Ribeiro, M. C. C. Da Silva, A. Gonçalves Dal-Bó and F. C. Giacomelli, *Langmuir*, 2019, **35**, 8060–8067.